COMMUNICATIONS IN COMPUTATIONAL PHYSICS
Vol. **6**, No. 1, pp. 1-23

Commun. Comput. Phys.
July 2009

REVIEW ARTICLE

Challenges and Technologies in Reservoir Modeling

Larisa V. Branets, Sartaj S. Ghai, Stephen L. Lyons and Xiao-Hui Wu*

ExxonMobil Upstream Research Company, 3120 Buffalo Speedway, Houston, TX 77098, USA.

Received 6 February 2008; Accepted (in revised version) 3 June 2008

Available online 13 November 2008

Abstract. Reservoir modeling is playing an increasingly important role in developing and producing hydrocarbon reserves. In this paper, we provide a brief overview of some main challenges in reservoir modeling, i.e., accurate and efficient modeling of complex reservoir geometry and heterogeneous reservoir properties. We then present modeling techniques we recently developed in addressing these challenges, including a method for generating constrained Voronoi grids and a generic global scale-up method. We focus on the Voronoi gridding method, which is based on a new constrained Delaunay triangulation algorithm and a rigorous method of adapting Voronoi grids to piecewise linear constraints. The global scale-up method based on generic flows is briefly described. Numerical examples are provided to demonstrate the techniques and the advantage of combining them in constructing accurate and efficient reservoir models.

AMS subject classifications: 37M05, 76S05, 86A60, 65M50, 65N50

Key words: Reservoir modeling, grid generation, grid adaptation, global scale-up.

Contents

*Corresponding author. *Email addresses:* larisa.v.branets@exxonmobil.com (L. V. Branets), sartaj.s.ghai@exxonmobil.com (S. S. Ghai), steve.lyons@exxonmobil.com (S. L. Lyons), xiao-hui.wu@exxonmobil.com (X.-H. Wu)

1 Introduction

The upstream oil industry involves finding hydrocarbon deposits, developing them, and producing the hydrocarbons for commercial use. Over the past few decades, numerous technological advances in the oil industry, e.g., remote detection and identification of hydrocarbons, extended reach drilling, and polymer flooding, have increased the success rate of finding reserves, made it possible to develop them and improved the recovery from existing resources. In addition, advances in computing capabilities have enabled geologists and engineers to model the reservoirs with increasing accuracy. In order to meet the ever increasing global hydrocarbon demand, heavy capital investments and continuous technological advances are required.

Various technologies used to understand a prospective reservoir provide information at many different scales. Core plugs are a few inches in size. Well logs can detect properties within a few feet around the well. Seismic imaging covers a huge volume, but its typical resolution is limited to a few meters vertically and tens of meters horizontally. Limited by time and capital, direct sampling of reservoir rock and fluid properties is sparse. Therefore, geologic interpretations based on seismic information and understanding of sedimentary processes are used to interpolate or extrapolate the measured data in order to yield complete reservoir descriptions. Information provided by these technologies is incorporated into reservoir models. Constructing reservoir models has become a crucial step in resource development as reservoir modeling provides a venue to integrate and reconcile all available data and geologic concepts.

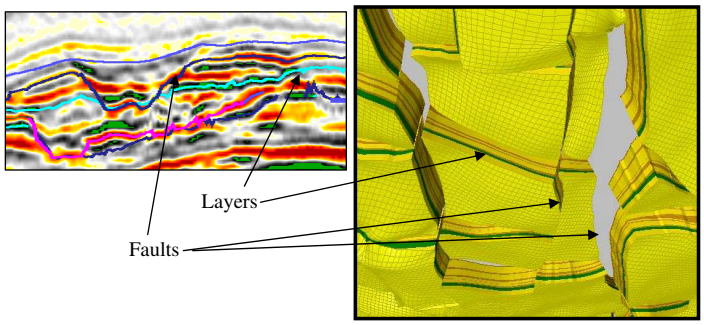

Figure 1: Subsurface structural geometry: faults and stratigraphic layers. Left: seismic image of subsurface. Right: reservoir model with multiple faults.

One of the key challenges in reservoir modeling is accurate representation of reservoir geometry, including the structural framework (i.e., horizons/major depositional surfaces that are nearly horizontal, and fault surfaces which can have arbitrary spatial size and orientation), and detailed stratigraphic layers (Fig. 1). The structural frameworks delineate major compartments of a reservoir and often provide the first order controls on in-place fluid volumes and fluid movement during production. Thus, it is important to model the structural frameworks accurately. However, despite decades of advances in

grid generation across many disciplines, grid generation for practical reservoir modeling and simulation remains a daunting task.

Specific challenges in grid generation for reservoir simulation arise from the complex structure of subsurface reservoir geometry (Fig. 1). Typical aspect ratio of reservoir dimensions, horizontal to vertical, can be several orders of magnitude. As a consequence, the aspect ratio of grid cell is usually 10 to 100. In this setting, 2.5D (prismatic) Voronoi grids, constructed by projection or extrusion of a 2D Voronoi grid in vertical or nearly vertical direction, are a natural choice for reservoir simulations. Prismatic grid cells can easily be constrained to resolve horizons or stratigraphic layer boundaries. Voronoi grids are much more flexible and adaptive than corner point grids commonly used in commercial reservoir simulators, generally providing much fewer grid cells for the same accuracy of geometry representation and simulation. They also help reduce the grid orientation effect on numerical solutions of fluid transport problems (Verma 1996). Although less problematic than corner point grids, generating 2.5D Voronoi grids is often very challenging in practice due to the constraints these grids have to honor, which include numerous (intersecting) faults, pinch-outs (areas where distinct horizons meet and continue as one surface, cf. Lyons et al. 2006), correlated heterogeneities (e.g., permeability extremes), and adaptive refinement as required for efficient and accurate flow simulations.

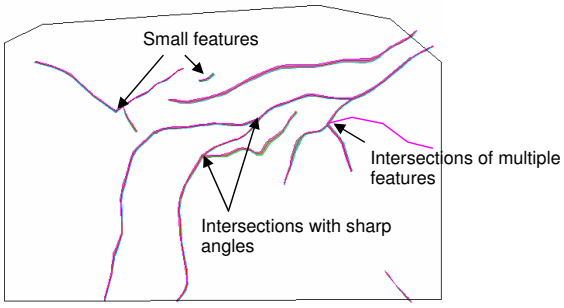

Figure 2: Top view of a faulted structural framework. Features shown are projections of faults.

In many practical situations, the challenges of accurately constraining and adapting the 2.5D Voronoi grid are associated with a 2D grid generation problem. To construct 2.5D grids, 2D grids are first generated on a planar projection of the reservoir domain, including all the constraining features such as faults and boundaries of the reservoir model (Fig. 2). The projected features provide constraints to the 2D grids. The 2D grids are then projected vertically (or along deviated lines) to account for (non-vertical) faults and yield a prismatic grid suitable for reservoir simulations (Gunasekera et al. 1997).

In this paper, we present novel approaches for generating adaptive, constrained 2D Delaunay and Voronoi grids. Since a constrained 2D grid resolves constraining features with cell edges, a constrained Delaunay triangulation (having vertices on the features) is *not* a dual of a constrained Voronoi grid (having cell centers away from the features). Constrained Delaunay triangulation algorithms is an active research area (see, e.g., Chew

1989, Ruppert 1995, Shewchuk 2002, Miller et al. 2003), whereas the constrained Voronoi grids have not been extensively studied in the literature. Fig. 2 shows some of the challenges in generating a constrained Voronoi grid, i.e., exactly honoring the small features, intersections of multiple features, and intersections of features at sharp angles.

Several techniques have been proposed to solve the problem of constrained Voronoi grid generation for accurate reservoir simulation. In a technique by Heinemann et al. (2003), the grid exactly honors polylines (i.e., faults) but fails to be Voronoi in the vicinity of the fault. This simplification makes the flow calculations less accurate. Approaches by Verma (1996) and Gunasekera (1997) always yield Voronoi grid cells but do not guarantee exact representation of the constraints. They fail to accurately constrain the Voronoi grid in the presence of challenging features indicated in Fig. 2.

Our new method for generating adaptive constrained Voronoi grids allows resolving the internal features exactly with the Voronoi cell faces while adapting the grid cell sizes to a specified density function. It overcomes the difficulties mentioned above (Fig. 2). The algorithm is based on constrained Delaunay triangulations and a novel protection area concept. We also developed a new algorithm for generating constrained Delaunay triangulations based on a grid smoothing algorithm and local feature capturing operations. This algorithm enables automatic adaptation of cell sizes to a target density distribution (including the cells near the constraints) while preserving Delaunay triangulation conforming to constraints.

Another major challenge in reservoir modeling is to accurately and efficiently represent reservoir heterogeneity at multiple scales. Typically fine-scale geo-cellular models consist of 10^6-10^8 cells. Geostatistical methods are often used to populate the models with piecewise constant properties that honor known and/or inferred statistics. A typical fine-scale model captures geologic variations on the order of a foot in the vertical direction and a few hundred feet in the areal directions. But, heterogeneities at smaller scales can have a significant impact on the reservoir performance (Coll et al. 2001; Honarpour et al. 1994). Therefore, accurate *scale-up* of the reservoir properties to the fine-scale model is required to capture the effect of sub-fine-scale heterogeneities (cf. Pickup et al. 2005).

In practice, the fine-scale models often need to be further coarsened for multi-phase flow simulations. This is especially true when many simulation runs are needed to quantify uncertainty, match production history, or to optimize reservoir management. Practical simulations are often conducted with about 10^5 cells. Thus, coarse simulation models are constructed from the fine-scale geo-cellular models through another scale-up process. Here, both coarsening of reservoir model grids, or up-gridding, and scale-up of reservoir properties are involved. In fact, the two processes can be coupled to optimize the simulation grids, so that effects of strong correlated heterogeneity on the multi-phase fluid transport can be accurately captured on significantly coarser models. A number of studies have demonstrated the effectiveness of this approach (Durlofsky et al. 1997, Stern and Dawson 1999, Li and Beckner 2000, and Prevost et al. 2005). See Durlofsky (2005) for a review of recent developments in this area.

Grid optimization requires both advanced grid generation algorithms described above and accurate and efficient scale-up of reservoir properties, especially permeability. To this end, we have developed a global scale-up method based on generic flow solutions (i.e., flows calculated from generic boundary conditions). This type of method was first proposed in the 1980s (White and Horne 1987). Its rigorous mathematical analysis was done only recently (Owhadi and Zhang 2007). Significant challenges existed in applying it to real reservoir models, which often contain difficult geometry such as faults and pinchouts, and complex connectivity due to irregular distributions of flow barriers. We have developed a suite of techniques to make the method practical (Lyons et al. 2006, Wu et al. 2007a, 2008, Stone et al. 2007). Our approach is different from existing global or local-global scale-up methods that use specific well-driven flows (see, e.g., Pickup et al. 1992, Nielson and Tveito 1998, Holden and Nielson 2000, Zhang et al. 2005, Chen and Durlofsky 2005, Wen et al. 2005). The motivation behind using generic flows is to generate coarse models suitable for practical simulations with active well management (i.e., boundary condition changes at the wells). When necessary, specific well-driven flows can still be used to improve the accuracy of the simulation models (Chen and Wu, 2007, Owahdi 2007).

We remark that alternative methods have been studied to capture the effects of heterogeneity on fluid transport. For example, the use of pseudo-functions has been studied over the past several decades (cf. Barker and Thibeau 1997). It still has difficulty dealing with process dependency of scale-up results and is not widely applied (but see Efendiev and Durlofsky (2003) and references therein for recent progresses). Multiscale methods developed over the past decade attempt to solve flow and transport problems on coarse and fine grids, respectively, and use multiscale basis functions to map solutions between grids (see, e.g., Hou and Wu 1997, Chen and Hou 2003, Jenny et al. 2003, Aarnes 2004, Efendiev et al. 2006). While promising, these methods also face challenges in terms of up-gridding (Aarnes et al. 2006) and incorporating global flow information (Efendiev et al. 2006, Owhadi and Zhang 2007). Again, strong correlated heterogeneities are a source of the challenges.

In this paper, we present our new gridding algorithm and the global scale-up method, with emphasis on the former. In Section 2 we present new approaches for generating 2D adaptive, constrained Voronoi grids and Delaunay triangulations. In Section 3 we briefly review our global scale-up method. Numerical examples are given in Section 4 to demonstrate the benefits of using these new modeling techniques, emphasizing on the interplay between grid generation and scale-up. Concluding remarks are given in Section 5.

2 Adaptive constrained grid generation

In this section, we present our novel approach for generation of adaptive, constrained Voronoi grids that resolve all the constraining features (projections of faults and bound-

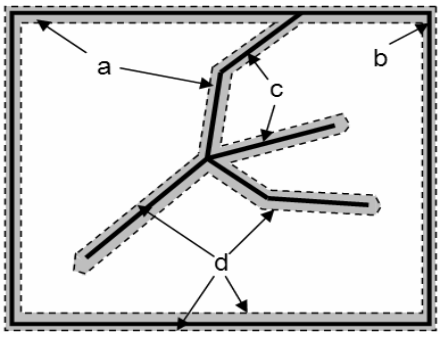

Figure 3: Use of protection areas (a) around domain boundary (b) and internal features (c) for constrained Voronoi grid generation. Voronoi grid honoring the features is known in (a) and boundaries of protection area (d) are the constraints for Delaunay triangulation.

aries) with cell edges and have cell sizes consistent with a target density specification (e.g., *a posteriori* error estimates, varying coefficients of the governing equations, such as permeability, etc.). In the following, we assume that prior to constrained grid generation, all constraining features in the model are approximated by a set of polylines or polygons yielding an input Planar Straight Line Graph (PSLG) P1.

Known approaches to constrained Voronoi grid generation (Verma 1996, Gunasekera 1997) distribute pairs of mirror-image points along the constraints to serve as centers of Voronoi cells thus forcing the face between each such pair of cells to lie on the constraint. This technique works for non-intersecting nearly straight constraints, but it is not sufficient for accurate gridding of polylinear, curved, and multiple intersecting constraints (recall challenges in Fig. 2).

The problem of a Voronoi grid generation is often regarded as a problem of constructing a Delaunay triangulation and vise versa due to the duality between the two grids. Introduction of the constraints, however, implies more complex dual relationships. By definition in (Chew 1989), the constrained Delaunay triangulation of a PSLG P1 includes only the edges and vertices of P1 as triangle edges and vertices, and it is as close to Delaunay triangulation as possible, meaning that it is Delaunay with regards to edges and vertices 'visible' or non-obstructed by the segments of P1. Constrained Delaunay triangulation is no longer a dual of the Voronoi diagram of P1. Delaunay refinement techniques (Ruppert 1995, Shewchuk 2002, Miller et al. 2003) with input PSLG P1 result in triangulations where all edges are Delaunay; however, the segments of P1 might be refined with the Steiner points added to achieve target triangle quality bounds and size/density specifications. The Voronoi grid dual to the refined Delaunay triangulation has its cell centers positioned on the P1 segments and, thus, is not a constrained Voronoi grid according to our definition.

We propose to reformulate a constrained Voronoi grid generation problem into a triangulation problem with the help of protection area concept (Fig. 3). Protection areas are

constructed around the constraining PSLG P1, such that their boundaries form another PSLG P2. The vertices of P2 serve as the centers of Voronoi cells and are constructed to give an exact representation of the internal features with the Voronoi grid edges. Constrained Delaunay triangulation or refinement can now be used to triangulate the complement of the protected areas with respect to the rest of the domain (with P2 as input). The challenge is to construct the protection areas in such a way that the union of Delaunay triangulations inside and outside of protection areas is also Delaunay and thus yields a consistent dual constrained Voronoi grid.

2.1 Constrained Voronoi grid generation: Protection areas

We introduce the technique for construction of protection areas using circles that addresses this challenge. Consider a polyline as P1 in Fig. 4a and assume that all segments in the polyline will be edges in the final Voronoi grid. Thus, the vertices on the polyline are vertices in the final Voronoi grid. We form intersecting circular disks around these vertices. The two intersection points of two neighboring circles will be vertices of the protection polygon and centers of Voronoi cells. Note that line segment AB is a perpendicular bisector of line segment CD. Additional points can be placed on the boundary of the union of the disks; no point is allowed inside that boundary. With these points, a protection polygon P2 is formed around the polyline.

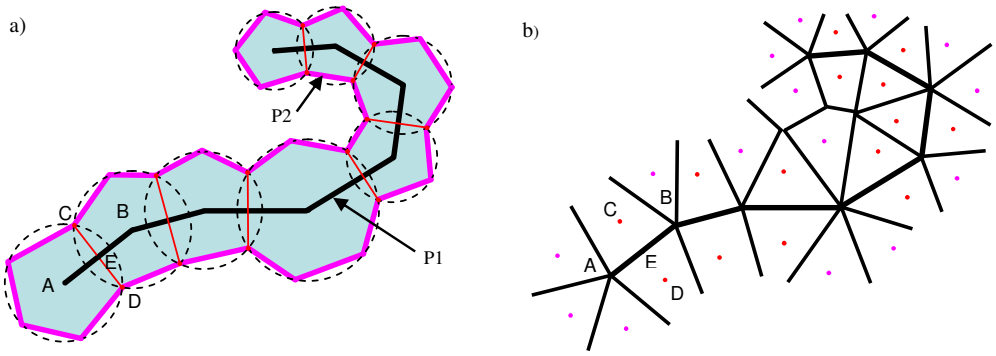

Figure 4: (a) A method to generate protection area bounded by P2 around a polyline P1 from circles. (b) Voronoi cell edges inside the protection area.

Inside the protection polygon P2, the Delaunay triangulation is not unique because triangles formed by points on the same circle share the same circumcenter (an example is point A). Since the protection area contains no point other than the ones on its boundary (vertices on the polyline P1 are not used in the triangulation), any Delaunay triangulation inside the protection area leads to the same unique Voronoi diagram whose edges include the line segments on the polyline (Fig. 4b).

In order to deal with the case of multiple polylines intersecting at one point, we use a similar idea as shown in Fig. 5. In this figure, four polylines (marked as Lines 1 to 4)

intersect at one point. We place points around the intersection on a circle centered at the intersection point (i.e., the inner circle in the figure). Thus, any Delaunay triangulation of the thick inner polygon produces triangles that share the same circumcenter, i.e., the intersection point.

To honor the intersecting polylines, the pair of points on the two sides of a polyline need to form mirror image with respect to the polyline, e.g., pairs A-B, A-C, D-E, and F-G in Fig. 5. For sharp angles such as the one formed between Line 1 and Line 2, it is preferable to place only one point on the dashed line bisecting the angle. This results in a triangular Voronoi cell to fit into the sharp angle. Again, no points are placed inside the inner circle.

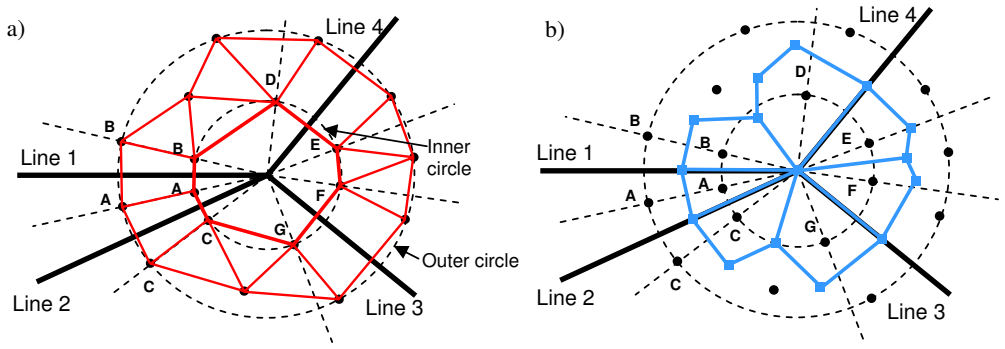

Figure 5: Generation of constrained Voronoi grid near an intersection point of multiple polylines: (a) triangulation and protection areas, (b) Voronoi cells.

Another circle can be used to further control the layout of Voronoi cells near the intersection, especially when sharp angles are present. Points are placed on this outer circle in the same way as those on the inner circle. However, points are allowed inside the outer circle. These points are used to control the sizes and shapes of Voronoi cells. Further away from the intersections, the method illustrated in Fig. 4 could be used to place points around the polylines.

When generating Delaunay triangulation in the complement of protection areas, no Steiner point is allowed inside the union of protection circles. Consequently, the union of triangulations inside and outside of protection areas will remain Delaunay and provide a dual constrained Voronoi grid.

In practice, the major difficulty in the suggested approach lies in defining the radii and spacing of protecting circles. The radii and spacing (refinement of P1) have to account for both local and global constraint geometry (e.g., curvature and distance to other constraints), as well as agree with a target mesh density specification. For example, it is preferable that the line segment formed by the intersections of two neighboring circles (e.g., CD in Fig. 4) to intersect the segment with end points being the centers of the circles (e.g., AB). This is not always possible if a long segment on the polyline neighbors two much shorter segments. In this case, the long segment needs to be refined. In another

example, if two constraints come close to each other but never intersect, the radii and spacing of the circles on both constraints need to be adjusted so that circles from different protection areas do not intersect or intersect exactly along the segments of P2 and the space left between the protection areas allows for generation of not-too-fine Delaunay triangles.

Similar problems of tying local and global constraint geometry with sizing and quality of mesh elements are being dealt with in Delaunay refinement algorithms. Thus, we employ Delaunay refinement in constructing protection areas. We first construct a Delaunay triangulation T conforming to the constraints P1 using a Delaunay refinement approach in Shewchuk (2002). This way, the triangles capture all the global and local information about the constraints. Then, the protection areas are constructed around the constraints by transforming the triangulation vertices on the constraints. Each point lying on the straight segment of P1 is replaced by the pair of protection points forming a mirror image of each other with respect to this segment (e.g., points C and D formed from boundary point E in Fig. 4). Each point lying at a corner or an intersection of several segments of P1 is replaced by a set of points placed on the circle around the intersection such as points A, $\cdots$, G in Fig. 5. The radius of the intersection circle or the distance between the old point and any protection point formed from it is determined as a fraction of minimum edge length (e.g., 0.25) of all triangle edges connected to the point on the constraint. Then, the protection circles are constructed from the protection points (and not the other way around).

Instead of generating a new Delaunay refinement in the complement of protection areas, we can reuse initial Delaunay triangulation T which only requires adjustment near the protection areas. The adjustment can be efficiently carried out by adding triangles where new points were introduced and an iterative swap of non-Delaunay edges. Thus, we have

Algorithm 2.1: Constrained Voronoi grid generation conforming to input PSLG P1

1. Generate Delaunay triangulation T0 conforming to PSLG P1.
2. Construct protection points from the vertices of T0 lying on the constraints. Use circles with radii determined form the edges of T0 adjacent to those constrained vertices.
3. Generate Delaunay triangulation T1 of the set of points consisting of the remaining (unconstrained) vertices of T0 and the protection points.
4. From T1 construct dual Voronoi mesh, which is conforming to PSLG P1.

An important advantage of the above method is that it conveniently lends itself to dynamic grid adaptation: initial constrained triangulation can be adapted or optimized, and the Voronoi grid updated through reconstruction of protection areas and localized re-triangulation.

2.2 Smoothing of constraints conforming Delaunay triangulation

For both Voronoi grids and Delaunay triangulations, Centroidal Voronoi Tessellation (CVT) algorithm (Du and Gunzburger 2002) can be used to optimize grid density according to a target function and even to include anisotropy. According to the CVT method, iterative smoothing procedure for Voronoi grids can be formulated as Lloyd's method where at each iteration, $k+1$, centers $\mathbf{Z}$ of Voronoi cells $V_i(\mathbf{Z})$ are repositioned to the mass centroids according to a density function ρ

$$\mathbf{Z}_i^{k+1} = \mathrm{T}_i(\mathbf{Z}^k) = \frac{\int_{V_i(\mathbf{Z}^k)} \mathbf{y}\rho(\mathbf{y})d\mathbf{y}}{\int_{V_i(\mathbf{Z}^k)} \rho(\mathbf{y})d\mathbf{y}} \tag{2.1}$$

and then re-triangulated. Lloyd' method converges to a CVT.

However, the CVT algorithm does not account for internal constraints. We propose a novel feature capturing procedure which, coupled with the Lloyd's iteration (2.1), provides an approach for smoothing Delaunay triangulation such that it remains Delaunay and conforms to features after each iteration. We then use this method for adaptive constrained Voronoi grid generation since it allows for cell size near boundary (or radius of the protecting circles) to be automatically determined from the density function.

Within each iteration of smoothing we combine the feature capturing procedure with node repositioning according to the Lloyd's iteration (2.1). Initial triangulation for smoothing can be any triangulation which includes vertices of the input PSLG P1, since it can be corrected by edge swap to honor the constraints and to have Delaunay unconstrained edges.

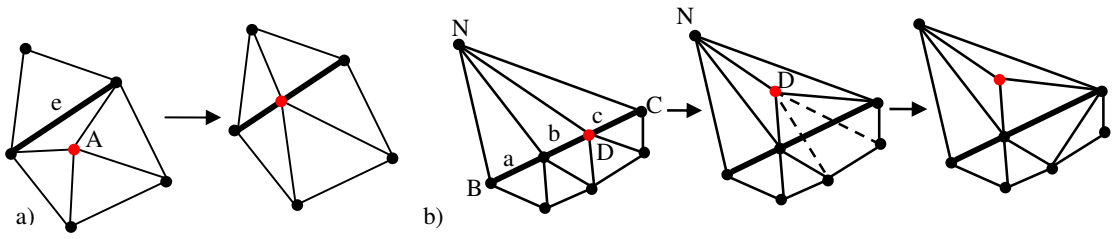

Figure 6: Feature capturing operations: (a) snapping interior point to the feature, (b) removing point from the feature into the interior.

Our feature capturing procedure is based on the two local operations illustrated in Fig. 6. In the first operation, an interior point (A) is snapped to a feature segment when it is a vertex of a triangle opposite a feature edge (e) and the angle at the vertex is obtuse. As a result of snapping, point A is projected onto the feature edge and edge (e) is swapped (Fig. 6a). In the second operation, a point (N) from a feature segment is moved into the interior when it is opposing feature edges (a, b, and c) on the same feature segment (BC) in at least 3 triangles and the summary of the angles at the point is acute. During the second operation, one of the edges connecting point N and a point (D) on the feature

segment is shrunk in half by moving point D into the interior. The movement is followed by swap of the edges connecting to point D which intersect the feature segment after the move of D (Fig. 6b).

Algorithm 2.2: Constraint preserving CVT smoothing of an input Delaunay triangulation

1. Loop through all the vertices in triangulation and snap the candidate points (e.g., A in Fig. 6a) to the features until there is no more candidate satisfying the snap condition formulated above is left; as a result, only acute angles are facing the feature edges.
2. Similarly, loop through all the vertices removing candidate points (e.g., N in Fig. 6b) from the features.
3. Correct triangulation by recursive edge-swap of interior non-Delaunay edges.
4. Reposition all points to the density-weighted centroids of their Voronoi regions (2.1) (points on the features are moved along the features only, as in Du and Gunzburger 2002).
5. Correct triangulation by recursive edge-swap of interior non-Delaunay edges.

2.3 Summary

To summarize, we have reformulated the constrained Voronoi grid generation problem in terms of requirements for triangulation. The key idea is the construction of protection areas around the constraints using circles. We showed that the protection circles can be constructed using Delaunay refinement techniques to capture both local and global constraint geometry information. Our approach is capable of addressing all the challenges of constrained Voronoi gridding shown in Fig. 2. We have also presented an algorithm for smoothing Delaunay triangulations so that they conform to constraining features. Thus, we can generate adaptive cell sizes everywhere in the domain, including on the constraints. The smoothing method can be used in combination with constrained Voronoi gridding algorithm for dynamic adaptation of constrained Voronoi grids.

3 Generic global scale-up

In this section, we briefly describe our global scale-up method to provide sufficient background for the reader to understand the numerical examples in Section 4. We refer the reader to Lyons et al. (2006), Stone et al. (2007), and Wu et al. (2007a, b, 2008) for more detailed descriptions as well as discussions on the challenges and our resolutions in applying the method to real models. These references also contain many numerical examples of the global scale-up method.

Let a detailed reservoir model be prescribed in a 3D domain Ω. We solve incompressible, single-phase Darcy flow equation with linear boundary conditions (White and

Horne 1987, Owhadi and Zhang 2005), i.e.,

$$\nabla\cdot(\mathbf{K}\nabla\mathbf{P})=\mathbf{0} \quad \text{in } \Omega; \qquad \mathbf{P}=\mathbf{x} \quad \text{on } \partial\Omega, \tag{3.1}$$

where $\mathbf{K}$ is fine-scale permeability and $\mathbf{P}$ is vector of three pressure solutions. Let $V\subset\Omega$ be a volume on which the effective permeability is to be calculated. We calculate constant tensor permeability via

$$\mathbf{K}_V^*=\langle\mathbf{K}\nabla\mathbf{P}\rangle_V\langle\nabla\mathbf{P}\rangle_V^{-1}, \tag{3.2}$$

where the angular brackets indicate volume averages over V. We call V a scale-up volume. Scale-up volumes can be grid blocks of a coarse grid or a set of random volumes. Results on the random volumes of same sizes can be used to estimate permeability statistics at that scale for building geo-cellular models. For finite-volume flow simulations, the effective permeability can be used to calculate transmissibilities (Gunasekera et al. 1997). Or better yet, one can scale-up the transmissibility directly. Wu et al. (2007a, 2008) presented a transmissibility scale-up formulation using generic flows. In this paper, permeability calculated on unions of two neighboring grid blocks are used to calculate the transmissibility, hence the additional harmonic average associated with traditional transmissibility calculation is avoided.

Note that the above volume average formulation (3.2) is the same as in local scale-up (see, e.g., Wu et al. 2002). However, the upscaled permeability tensor is not symmetric in general, especially when the scale of permeability heterogeneity is large compared to the size of a scale-up volume. The lack of symmetry can be explained by the lack of symmetry of the multiscale finite element method corresponding to the scale-up formulation (Wu et al. 2008).

4 Numerical examples

In this section, we present several examples of the gridding and scale-up methods described in the previous sections. Examples of constraint Delaunay and Voronoi grids are given first. Then, we show the impact of global scale-up in coarsening fine-scale models. Next, we apply adaptive gridding and global scale-up to a channelized reservoir model and demonstrate the advantage of this powerful combination.

4.1 Adaptive constrained 2D grid generation

First, we demonstrate the performance of our adaptive, constrained 2D grid generation methods and their ability to accurately honor the complex constraint geometry while adapting grid cell size to a given density function. In this section, we illustrate only the gridding capabilities (no upscaling or simulation is performed) on several examples representative of realistic settings for reservoir simulation gridding.

Fig. 7 shows adaptive Delaunay (Figs. 7a,b) and Voronoi (Figs. 7c,d) grids generated in a rectangular domain with polylinear constraints (in bold). The constraints do not

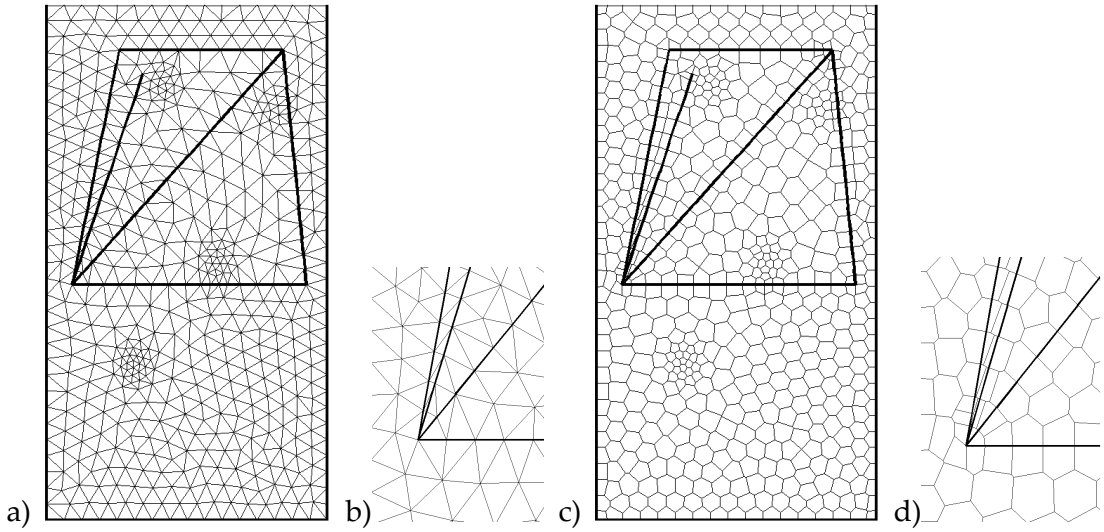

Figure 7: Domain with multiple internal constraints and near-well refinement density specification. (a) Adaptive constrained Delaunay triangulation and (b) zoom-in on the multiple feature intersection; (c) Adaptive constrained Voronoi grid and (d) zoom-in on the multiple feature intersection.

represent realistic reservoir geometry; they are used to demonstrate how our algorithms handle complex intersection of multiple features at sharp angles. A grid density function is also specified; it is the sum of several Gaussian functions with peaks centered at different points, so that the grids are refined near those points. Similar density functions can be used to refine grids around wells in real reservoir models. Clearly, our algorithms accurately resolve the constraints as well as adapt to the density distribution.

In Fig. 8, we use a 2D domain with internal features obtained from the projection of a faulted geological framework. The fault traces are approximated by a set of polylines (shown in bold in Figs. 8b and 8c). In this case, the density function is determined from the isotropic permeability field K shown in Fig. 8a. More specifically, $\rho = \{1, \text{if K} \leq 50\text{md; K, otherwise}\}$. Note that adapting cell sizes to permeability distribution is used here only to demonstrate the ability of our algorithm to handle discrete target density functions; it is not necessarily a good grid adaptation strategy in general. Figs. 8b and 8c illustrate the resulting adaptive Delaunay and Voronoi grids respectively which exactly resolve all the features with cell faces while providing varying cell sizes according to both feature geometry and density distribution.

As mentioned in the introduction, sometimes explicit representation of strong heterogeneities, especially correlated ones, is required to capture their effect on multi-phase flow and transport. An example is shown in Fig. 9 (see Section 4.3 for another example with flow simulation comparisons). Here, instead of adapting grid cell sizes to a density distribution defined from permeability (as in Fig. 8), we explicitly constrain the grid to the edges corresponding to high gradients in the permeability field. Permeability map

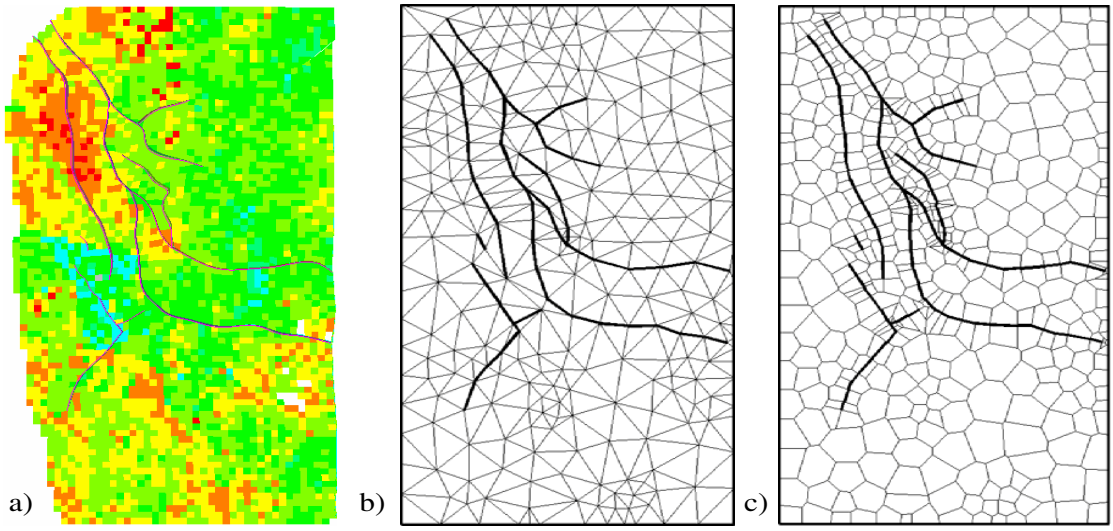

Figure 8: (a) Permeability in a hydrocarbon reservoir: logarithmic scale, high values in red, low in blue (range 10^{-5}-5000md); (b) Adaptive constrained Delaunay triangulation; (c) Adaptive constrained Voronoi grid.

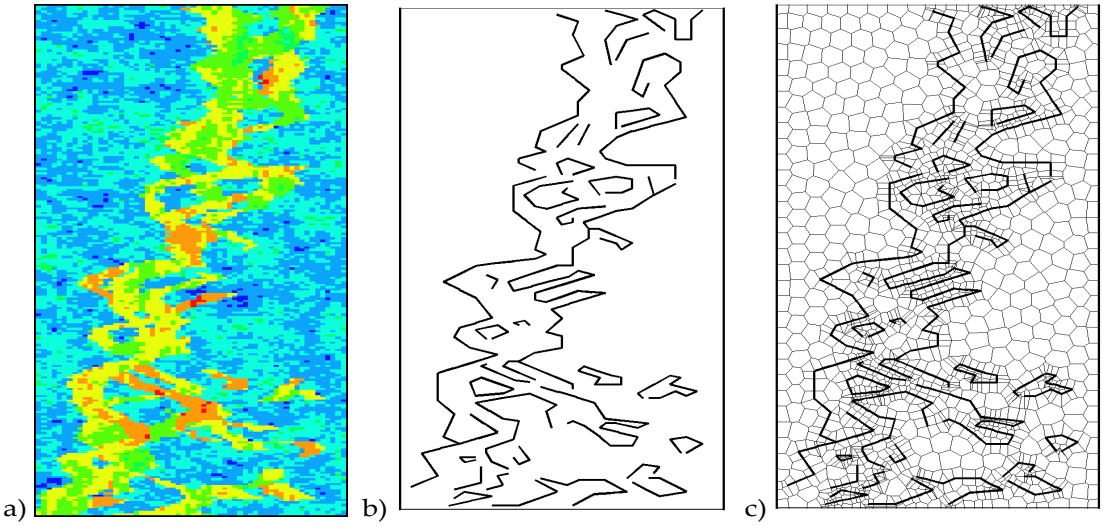

Figure 9: (a) Permeability in a SPE10 layer: logarithmic scale, high values in red, low in blue; (b) Edges constraining channel feature; (c) Constrained Voronoi grid.

for this example (Fig. 9a) is taken from a layer of the SPE10 model (Christie and Blunt, 2001) with a channel structure. The layer has 13200 cells. Fig. 9b shows a PSLG obtained from this permeability map using an edge detection algorithm. Fig. 9c shows the constrained Voronoi grid (1626 cells) conforming to this complex graph of linear features. Notice that smaller cell sizes near the constraints are determined automatically and are

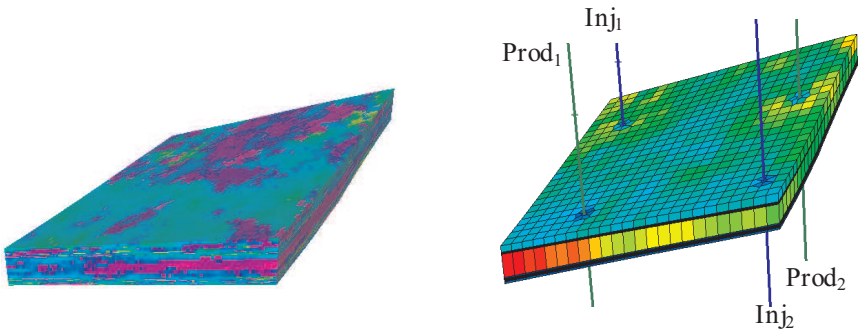

Figure 10: A fine-scale model for part of the Hugoton field (left) and a coarse simulation grid (right) with grid refinement near wells. Both models have been exaggerated vertically by a factor of 100 for display.

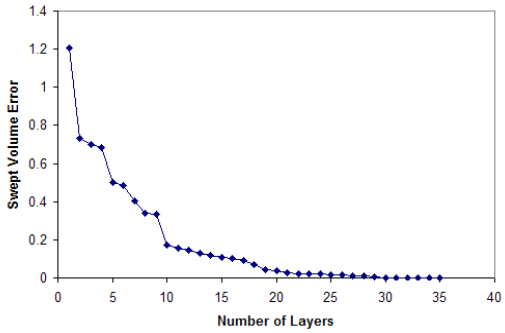

Figure 11: Estimated swept volume errors for different number of simulation layer.

influenced by both local and global information about the constraint geometry. Voronoi grid conforming to dynamic properties of flow solution (e.g., streamlines) can be constructed in a similar manner, resulting in flow-based Voronoi grid. Choice of controls on Voronoi grid might depend on particular problem, but it should always address the goal of achieving optimal balance between the accuracy of the flow solution and the number of degrees of freedom (grid cells) required to obtain this solution. This will be illustrated in the examples of Section 4.3.

4.2 Impact of up-gridding and global scale-up[†]

In this example, we examine the impact of degree of coarsening and global scale-up on building accurate and efficient simulation models. We use a small part of a fine-scale carbonate model built for the Hugoton field (see Fig. 10 and Dubois et al. 2006a, b). The model has $120\times120\times35$ cells and a permeability contrast of about 9 orders of magnitude, with the lowest permeability being 10^{-4}md. In the following, we investigate the impact of scale-up methods and up-gridding in both areal and vertical directions on the accuracy

[†]Portions of this material have been previously published in X. H. Wu et al. (2007c).

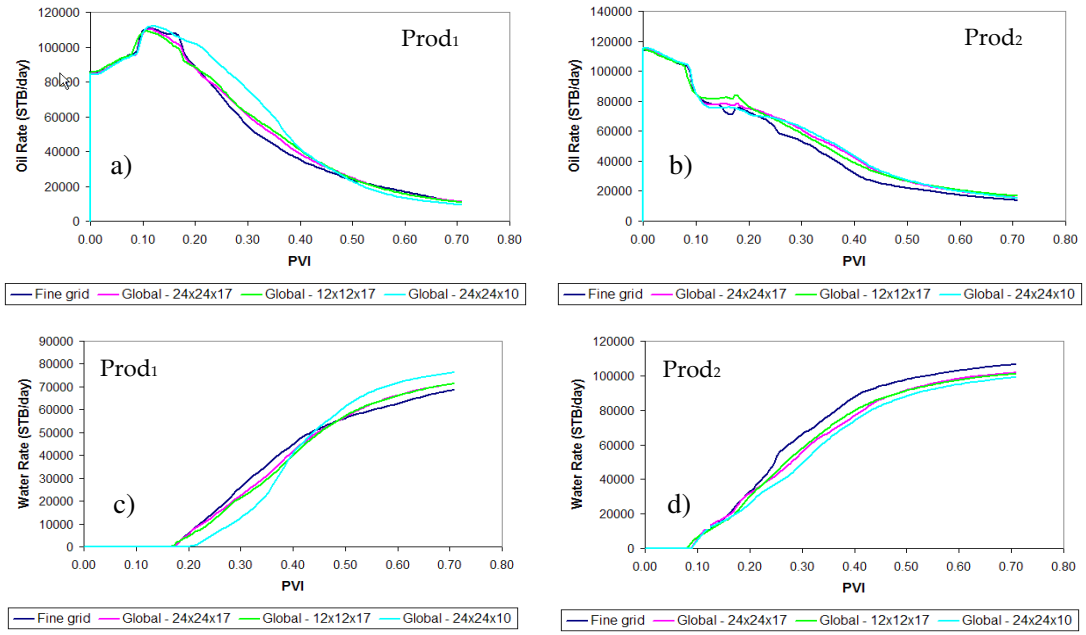

Figure 12: Comparison of oil and water rates calculated on the fine grid and three different coarse grids at the two producers. All models are scaled up using generic global flow solutions.

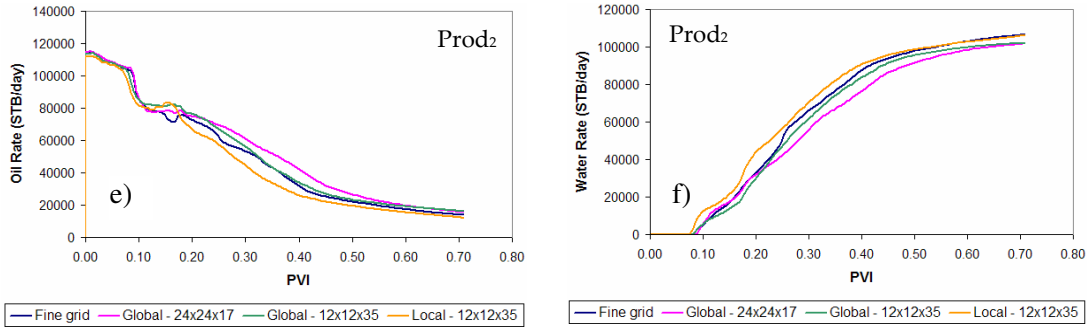

Figure 13: Comparison of oil and water rates calculated on the fine grid and two different coarse grids at Prod_2. Both global and local scale-up methods are used on the $12\times12\times35$ grid

of the coarse simulation models.

The layering for the simulation grid is important due to strong heterogeneity in the vertical direction (Fig. 10). Using an optimum layering technique (Stern and Dawson 1999), we can analyze the number of layers required without solving fine-scale flow solutions. Fig. 12 shows estimated swept volume error versus the number of simulation layers. Clearly, the error increases more rapidly beyond 10 layers. Based on this analysis, we test models with 10 or more layers.

The simulation models in the tests below have four vertical wells, two water injectors

(Inj_1 and Inj_2) and two producers ($Prod_1$ and $Prod_2$). Fig. 10 shows a model with 17 layers, which are chosen by using the optimum layering algorithm of Stern and Dawson (1999). A 5×5 areal coarsening is used in that model, except near the wells where smaller grid blocks are used to better represent the flow near the wells (Fig. 10, right). Thus, the grid dimension is approximately $24\times24\times17$. The models are scaled up using generic global flow solutions calculated on the fine-scale sector model. For the simulation, we fixed the injection rates of both injectors. For the producers, we fixed their bottom-hole pressures. The fluids are assumed to be incompressible and the capillary pressures are ignored.

Fig. 12 shows the comparison of water and oil rate at the two producers for three different coarse grids. It is evident from Figs. 12a and 12c that the coarse model with 10 layers is insufficient to capture the water breakthrough. The results with 17 layers are better. This is consistent with the swept volume error estimates shown in Fig. 11, where the swept volume error for 10 layers is about twice as much as the error for 17 layers. Moreover, the model with $12\times12\times17$ grid performs similarly to the model with finer areal grids. However, Figs. 12b and 12d indicate that more simulation layers are required to further improve the results at $Prod_2$. This observation is confirmed by the Fig. 13, which shows additional simulation results on a $12\times12\times35$ grid (no scale-up in the vertical direction and a factor of 100 scale-up in the areal direction as compared to the fine-scale sector model).

Table 1: Summary of simulation errors on the 12x12x35 grid due to global and local scale-up.

	Global Scale-up (% error)		**Local Scale-up (% error)**	
Wells	$Prod_1$	$Prod_2$	$Prod_1$	$Prod_2$
Initial Rate	-0.24	0.18	1.57	-1.19
Cum. Oil	3.68	3.88	-5.76	-6.93
Cum. Water	-4.00	-3.96	10.89	4.44
Wells	Inj_1	Inj_2	Inj_1	Inj_2
Average Pressure	-3.31	10.7	17.9	62.2

For comparison, the $12\times12\times35$ grid was scaled up by using a local method (Khan and Dawson, 2001). The simulation result obtained on this model is shown in Fig. 13. The errors in flow rates, pressure, and cumulative productions due to local and global scale-up are given in Table 1. We observe that errors in the initial production rate, which measure the accuracy of single-phase scale-up in terms of inter-well connectivity, are small. Local scale-up gives slightly larger errors in cumulative fluid productions, which is consistent with Fig. 13. However, local scale-up gives much larger error in the time-averaged injector pressures, implying that the local scale-up failed to capture the overall connectivity of the fine-scale model.

In addition to the above tests, we also used a uniform hexagonal grid with similar areal cell size and the same number of layers to repeat the above simulations. With global scale-up, little change in model accuracy was found. Thus, in this case, the accuracy of

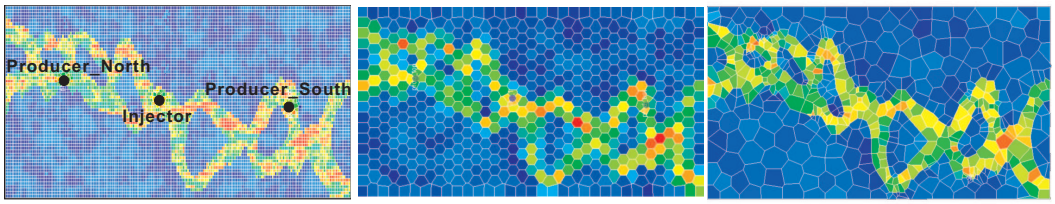

Figure 14: Fine-grid (left), uniform hexagonal grid (center), and adaptive grid (right) used in the example.

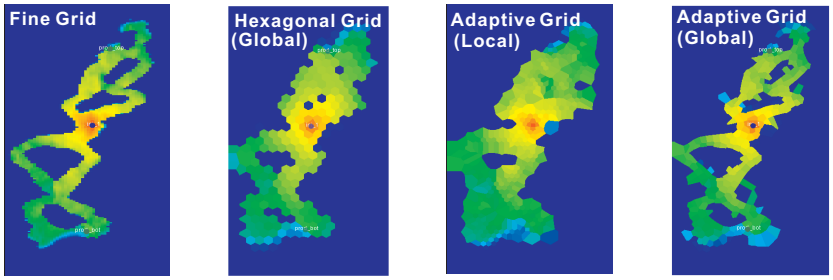

Figure 15: Comparison of water saturation profiles on different grids after 8000 days of water injection.

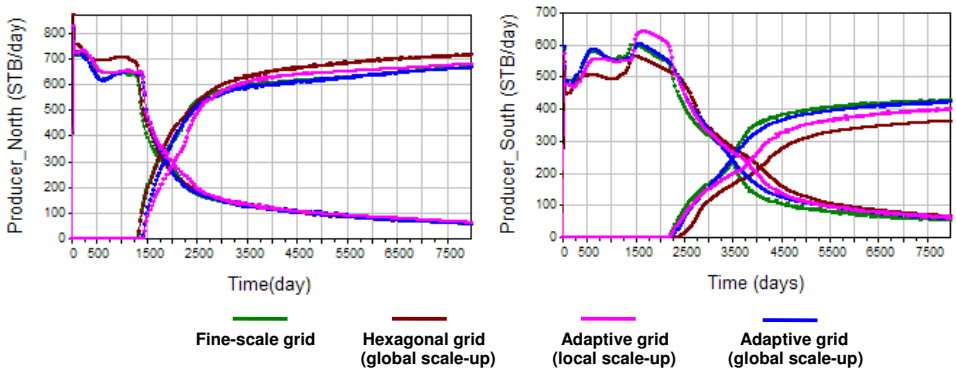

Figure 16: Oil production rates at the North and South wells.

global scale-up is insensitive to the areal grids, which is expected given the lack of areal features in the permeability distribution (Fig. 10). However, this is not always the case as shown by the next example.

4.3 Adaptive gridding with global scale-up‡

In the above example, we showed that for carbonate systems, vertical layering is important to accurately capture flow solutions on the coarse-grid and when global scale-up is used, the shape/size of the areal grid does not affect the flow solution significantly. However, for systems with strong, anisotropically correlated, areal heterogeneity, e.g.,

‡Portions of this material have been previously published in Wu et al. (2007c).

channelized features, the shape and size of the areal grid becomes important to obtain an accurate scale-up.

Here, we consider a fine-scale model with $60\times220\times3$ cells. Three vertical wells, one water injector with constant injection rate and two producers with fixed bottom-hole pressure are placed in the reservoir (Fig. 14).

To remove the effect of layering only areal coarsening is performed in the simulation models. We created two coarse-scale models, one model with uniform hexagonal grids (650 cells per layer, 3 layers) and the other with a Voronoi grid adapted to the channels in the fine-scale model (649 cells per layer, 3 layers) (Fig. 14). A number of parameters can be used to constrain the Voronoi grids. In this example, we have used the static permeability property in the fine-scale model. One can also use global flows calculated on the fine-scale model, such as the generic flows used by global scale-up or specific well-driven flows for a given production scenario, to further improve the accuracy of the coarse model. In this case, the flow solutions are strongly correlated to the permeability. Thus, using the static property is sufficient for upgridding purpose. The hexagonal grid was chosen because it typically provides better inter-well and overall model connectivity for channelized systems in comparison to a rectangular grid (Wu et al. 2007a).

We apply global scale-up on the uniform hexagonal grid and both global and local scale-ups on the adaptive Voronoi grid. Water flooding simulations are performed on these models, where the fluids are assumed to be incompressible and the capillary pressure is ignored. The simulation results of these models are then compared with the fine-scale simulation in Figs. 15 and 16. These figures show clearly that the adaptive grid with global scale-up matches the water saturation profile calculated on the fine-scale model closely, whereas the adaptive grid with local scale-up shows much larger sweep volume than the fine-scale model. In this case, the linear boundary condition used by the local scale-up smears the channel boundaries, even though these boundaries are precisely represented by the grid. The smearing occurs in another form on the uniform, hexagonal grid; it is caused by the mixing of high and low permeabilities in the coarse-grid cells. Visually, the smearing clearly affects the swept volume. More subtly, the smearing introduces larger errors in the initial production rates, as shown in Fig. 16.

Table 2: Water breakthrough and cumulative production error (in comparison to the fine-scale results) in the two producers.

	Water breakthrough (days)		**Cumulative production (% error)**			
			Oil		**Water**	
Grid:	**North**	**South**	**North**	**South**	**North**	**South**
Fine-scale	1308	2100	–	–	–	–
Hexagonal (global scale-up)	1278	2191	5.7	5.4	6.6	23.6
Adaptive (local scale-up)	1370	2100	6.9	7.1	1.0	11.7
Adaptive (global scale-up)	1370	2100	2.5	4.7	2.0	3.3

The difference in these models can also be studied by observing the water breakthrough and cumulative production by the two producers (Table 2). The combination of adaptive grid and global scale-up provides better accuracy than other combinations, especially for the water production in the South producer. Thus, to accurately capture the fine-scale displacement process on a highly channelized reservoir on coarse-grids, it is important to generate coarse-grids that closely represent the channel geometry and to use accurate scale-up methods.

5 Concluding remarks

In this paper, we gave an overview of reservoir modeling challenges, emphasizing on the modeling of complex geometry and heterogeneous properties of reservoir. We then presented some techniques we recently developed to address these challenges. Our approach is to combine advanced gridding techniques with an accurate global scale-up method in constructing coarse simulation models from fine-scale geo-cellular models. For gridding, we have developed new algorithms for generating adaptive constrained Voronoi grids in 2D planes. These algorithms can be used to generate adaptive 3D prismatic grids suitable for reservoir simulations. Several examples were presented to demonstrate the effectiveness of the algorithms both in terms of honoring polylinear constraints and specified density functions. In addition, we presented a brief overview of a generic global scale-up method we developed and numerical examples demonstrating its accuracy. In particular, we showed that combining the adaptive constrained Voronoi gridding with global scale-up is especially effective in capturing the effect of strong correlated heterogeneities such as sinuous channels.

While significant progresses have been made over the past few years in the area of gridding and scale-up (see e.g., Durlofsky 2005), including those presented in this paper, significant practical challenges remain to be resolved for reservoir modeling. Among them, *accurate* and *effective* representation of reservoir geometry and heterogeneity will be on the top of the list in the foreseeable future. This is because reservoir descriptions are becoming more detailed and complex due to better resolutions in remote sensing (e.g., seismic imaging) technology, increasing amount of data collected from producing fields (e.g., via permanent down-hole gauges), and better geologic understanding. However, not every geologic detail matters to the prediction of fluid movement in practice. Therefore, the perennial challenge in reservoir modeling is to strike the balance between explicit representation of reservoir geometry and heterogeneity through gridding and accurate capture of their effects on multi-phase flows via scale-up.

References

[1] J.E. Aarnes, On the use of a mixed multiscale finite element method for greater flexibility and increased speed or improved accuracy in reservoir simulation, Multiscale Model. Simul., 2 (2004), 421-439.

[2] J. E. Aarnes, S. Krogstad, and K.-A. Lie, A hierarchical multiscale method for two-phase flow based upon mixed finite elements and nonuniform coarse grids, Multiscale Model. Simul., 5 (2006), 337-363.
[3] J. W. Barker and S. Thibeau, A critical review of the use of pseudorelative permeabilities for upscaling, SPE Reservoir Engineering, 12 (1997), 138-143.
[4] A. Bowyer, Computing Dirichlet tessellations, Comput. J., 24 (1981), 162-166.
[5] Y. Chen and L. J. Durlofsky, Adaptive local-global upscaling for general flow scenarios in heterogeneous formations, Transport Porous Media, 62 (2006), 157-185.
[6] Y. Chen and X. H. Wu, Upscaled modeling of well singularity for simulating flow in heterogeneous formations, Comput. Geosciences, 12 (2008), 29-45.
[7] Z. Chen and T. Y. Hou, A mixed multiscale finite element method for elliptic problems with oscillating coefficients, Math. Comput., 72 (2003), 541-576.
[8] L. P. Chew, Constrained Delaunay triangulation, Algorithmica, 4 (1989), 97-108.
[9] M. A. Christie and M. J. Blunt, Tenth SPE comparative solution project: A comparison of upscaling techniques, SPE Reservoir Evaluation & Engineering, 4 (2001), 308-317.
[10] C. Coll, A. H. Muggeridge and X. D. Jing, A new method to upscale waterflooding in heterogeneous reservoirs for a range of capillary and gravity effects, SPE 74139 (2001).
[11] M. K. Dubois, A. P. Byrnes, S. Bhattacharya, G. C. Bohling, J. H. Doveton and R. E. Barbra, Hugoton Asset Management Project (HAMP): Hugoton geomodel final report, `http://www.kgs.ku.edu/PRS/publication/2007/OFR07_06/index.html` (2006a).
[12] M. K. Dubois, A.P. Byrnes, G.C. Bohling and J.H. Doveton, Multiscale geologic and petrophysical modeling of the giant Hugoton gas field (Permian), Kansas and Oklahoma, P. M. Harris and L. J. Weber, eds., Giant reservoirs of the world: From rocks to reservoir characterization and modeling: American Association of Petroleum Geologists Memoir 88 (2006b), 307-353.
[13] Q. Du and M. Gunzburger, Grid generation and optimization based on centroidal Voronoi tessellations, Appl. Math. Comput., 133 (2002), 591-607.
[14] L. J. Durlofsky, Upscaling and gridding of fine scale geological models for flow simulation, Proc. of 8th Intl. Forum on Res. Sim., Stresa, Italy, June 20 - 25, 2005.
[15] L. J. Durlofsky, R. C. Jones and W. J. Milliken, A nonuniform coarsening approach for the scale up of displacement processes in heterogeneous media, Adv. Water Resources, 20 (1997), 335-347.
[16] Y. Efendiev and L. Durlofsky, A generalized convection-diffusion model for subgrid transport in porous media, Multiscale Model. Simul., 1 (2003), 504-526,.
[17] Y. Efendiev, V. Ginting, T. Hou and R. Ewing, Accurate multiscale finite element methods for two-phase flow simulations, J. Comput. Phys., 220 (2006), 155-174.
[18] D. Gunasekera, J. Cox and P. Linsey, The generation and application of K-orthogonal grid systems, SPE paper 37998 (1997).
[19] Z. E. Heinemann and G. F. Heinemann, Gridding techniques for reservoir simulation, Proc. 7th Intl. Forum on Res. Sim., Schlosshotel Buhlerhohe, Germany, June 23-27, 2003.
[20] M. M. Honarpour, A. S. Cullick and N. Saad, Influence of small-scale rock laminations on core plug oil/water relative permeability and capillary pressure, SPE 27968 (1994).
[21] L. Holden and B. F. Nielson, Global upscaling of permeability in heterogeneous reservoirs: Tthe Output Least Squares (OLS) method, Transport Porous Media, 40 (2000), 115-143.
[22] T. Y. Hou and X-H. Wu, A multiscale finite element method for elliptic problems in composite materials and porous media, J. Comput. Phys., 134 (1997), 169-189.
[23] P. Jenny, S. H. Lee and H. A. Tchelepi, Multi-scale finite-volume method for elliptic problems

in subsurface flow simulation, J. Comput. Phys., 187 (2003), 47-67.
[24] S. A. Khan and A. G. Dawson, Method of upscaling permeability for unstructured grids, U.S. Patent No. PCT/US00/17101 (2000), Dec. 28.
[25] S. Kocberber, An automatic unstructured grid generation system for geologically complex reservoirs, SPE paper 28245 (1994).
[26] D. Li and B. Beckner, Optimal uplayering for scaleup of multimillion-cell geologic models, SPE paper 62927 (2000).
[27] R. Lohner and J. Cebral, Generation of non-isotropic unstructured grids via directional enrichment, Int. J. Numer. Methods Engineering, 49 (2000), 219-232.
[28] S. L. Lyons, R. R. Parashkevov and X. H. Wu, A family of H1-conforming finite element spaces for calculations on 3D grids with pinch-outs, Numer. Linear Algebra Appl., 13 (2006), 789-799.
[29] G. L. Miller, S. E. Pav and N. J. Walkington, When and why Ruppert's algorithm works, Proc. 12th Intl. Meshing Roundtable (2003), 91-102.
[30] B. F. Nielson and A. Tveito, An upscaling method for one-phase flow in heterogeneous reservoirs. A Weighted Output Least Squares (WOLS) approach, Comput. Geosciences, 2 (1998), 93-123.
[31] H. Owhadi and L. Zhang, Metric based up-scaling, Comm. Pure Appl. Math., 60 (2007), 675-723.
[32] G. E. Pickup, K. D. Stephen, J. Ma, P. Zhang and J. D. Clark, Multi-stage upscaling: selection of suitable methods, Transport Porous Media, 58 (2005), 191-216.
[33] G. E. Pickup, J. L. Jensen, P. S. Ringrose and K. S. Sorbie, A method calculating permeability tensors using perturbed boundary conditions, 3rd European Conference on the Mathematics of Oil Recovery, Delft, The Netherlands, 1992.
[34] M. Prevost, F. Lepage, L. J. Durlofsky and J.-L. Mallet, Unstructured 3D gridding and upscaling for coarse modelling of geometrically complex reservoirs, Petroleum Geoscience, 11 (2005), 339-345.
[35] J. Ruppert, A Delaunay refinement algorithm for quality 2-dimensional mesh generation, J. Algorithms, 18 (1995), 548-585.
[36] J. R. Shewchuk, Delaunay refinement algorithms for triangular mesh generation, Comput. Geometry: Theory and Applications, 22 (2002), 21-74.
[37] D. Stern and A. G. Dawson, A technique for generating reservoir simulation grids to preserve geologic heterogeneity, SPE paper 51942 (1999).
[38] M. T. Stone, X. H. Wu, R. R. Parashkevov and S. L. Lyons, Challenges and solutions in global flow based scaleup of permeability: isolated flow bodies, SPE paper 106084 (2007).
[39] S. K. Verma, Flexible grids for reservoir simulation, PhD thesis (1996), Stanford University.
[40] X. H. Wen, and J. J. Góez-Hernádez, Upscaling hydraulic conductivities in heterogeneous media: An overview, Journal of Hydrology, 183 (1996), ix-xxxii.
[41] X. H. Wen, L. J. Durlofsky and Y. Chen, Efficient three-dimensional implementation of local-global upscaling for reservoir simulation, SPE paper 92965 (2005).
[42] C. D. White and R. N. Horne, Computing absolute transmissibility in the presence of fine-scale heterogeneity, SPE paper 16011 (1987).
[43] X. H. Wu, Y. R. Efendiev and T. Y. Hou, Analysis of upscaling absolute permeability, Discrete and Continuous Dynamical Systems, Series B, 2 (2002), 185-205.
[44] X. H. Wu, and R. R. Parashkevov, Effect of grid deviation on flow solutions, SPE paper 92868 (2005).
[45] X. H. Wu, M. T. Stone, R. R. Parashkevov, D. Stern and S. L. Lyons, Reservoir modeling with

global scale-up, SPE paper 105237 (2007a).
[46] X. H. Wu, S. S. Ghai, M. T. Stone, R. R. Parashkevov and S. L. Lyons, Improving reservoir modeling with global scale-up, IPTC paper 11335 (2007b).
[47] X. H. Wu, R. R. Parashkevov, M. T. Stone and S. L. Lyons, Global scale-up on reservoir models with piecewise constant permeability field, J. Algorithms Comput. Tech., 2 (2008), 223-247.
[48] P. Zhang, G. E. Pickup and M. A. Christie, A new upscaling approach for highly heterogeneous reservoirs, SPE paper 93339 (2005).